

# Anyon optics with time-of-flight interferometry of double-well-trapped interacting ultracold atoms

Constantine Yannouleas\* and Uzi Landman†

*School of Physics, Georgia Institute of Technology, Atlanta, Georgia 30332-0430*

(Dated: 10 December 2018)

The subject matter of bianyon interference with ultracold atoms is introduced through theoretical investigations pertaining to the second-order momentum correlation maps of two anyons (built upon spinless and spin-1/2 bosonic, as well as spin-1/2 fermionic, ultracold atoms) trapped in a double-well optical trap. The two-particle system is modeled according to the recently proposed protocols for emulating an anyonic Hubbard Hamiltonian in ultracold-atom one-dimensional lattices. Because the second-order momentum correlations are mirrored in the time-of-flight spectra in space, our findings provide impetus for time-of-flight experimental protocols for detecting anyonic statistics via interferometry measurements of massive particles that broaden the scope of the biphoton double-slit interferometry of quantum optics.

*Motivation.* Emulations of condensed-matter many-body physics [1, 2] and of optical biphoton interferometry [3–9] with ultracold atoms in optical traps and lattices, as well as quantum simulations of many-body phenomena using nonlinear-optics platforms (e.g., coupled resonator arrays or waveguide lattices) [10–17] constitute complimentary branches of research that have witnessed explosive growth in the last two decades. A great promise of these emerging research branches rests with their potential for achieving actual simulations of exotic synthetic particles that have been theoretically proposed in many-body and elementary-particle physics, but have been problematic to realize within the experimental framework of traditional condensed-matter and high-energy subfields of physics.

In this context, the properties and probable detection of synthetic particles, proposed initially in two dimensions and referred to as anyons [18, 19], that obey nontrivial particle-exchange statistics interpolating between the familiar bosonic and fermionic ones, continues to be an intensely active field of theoretical and experimental research across several disciplines of physics; see, e.g., in the context of quantum computing [20, 21], noninteracting ultracold anyonic atoms in harmonic traps [22], and quasiholes in a fractional quantum Hall state of ultracold atoms [23]. In particular, of great interest for the scope of this paper are theoretical [14, 15] and experimental [16] studies for simulating anyonic NOON states with photons in waveguide lattices.

Recently, going beyond the case of two-dimensional space, a propitious direction for the simulation of *massive* anyons opened when several experimental protocols (based on a fractional Jordan-Wigner transformation) were advanced [24–26], showing that ultracold neutral atoms trapped in *onedimensional* optical lattices can offer an appropriate substrate for the implementation of anyonic statistics. In particular, an anyonic Hubbard

model (related to spinless bosons) was formulated and, in analogy with condensed-matter themes, the influence of 1D anyonic statistics on ground-state phase transitions was explicitly studied in these [24–26] and subsequent publications [27–29].

Here, taking fully into account the interparticle interactions, we introduce the subject matter of 1D anyonic matter-wave interferometry with ultracold atoms and establish analogies with the quantum-optics biphoton interferometry of massless and noninteracting photons. To this effect, we present theoretical investigations pertaining to the second-order momentum correlation maps of two anyons (built upon (i) spinless and (ii) spin-1/2 bosonic, as well as (iii) spin-1/2 fermionic, ultracold atoms) trapped in a double-well optical trap. The two-particle system is modeled by an anyonic Hubbard Hamiltonian. Because the second-order momentum correlations are mirrored in the time-of-flight spectra in space, our findings provide impetus for time-of-flight experimental protocols for probing anyonic statistics via interferometry measurements of massive particles that broaden the scope of the biphoton double-slit interferometry of quantum optics.

In congruence with related studies of photonic anyons [14–16], a main finding of our study is that the anyonic signature in the two-particle interferometry maps reflects the appearance of a generalized NOON state as a major component in the entangled wave function of the ultracold atoms trapped in the double well. This NOON-state component is of the form  $(|2, 0\rangle \pm e^{i\theta}|0, 2\rangle)/\sqrt{2}$ , where  $\theta$  is the statistical angle determining the commutation (anticommutation) relations for the anyonic exchange (see below).

*Anyonic exchange.* For spin-1/2 (i.e., two-flavor) anyons, the annihilation and creation operators are denoted as  $a_{j,\sigma}$  and  $a_{j,\sigma}^\dagger$ , where the index  $j = 1, 2$  (or equivalently  $j = L, R$ ) denotes the left-right well (corresponding Hubbard-model site). These operators obey anyonic

---

\* Constantine.Yannouleas@physics.gatech.edu

† Uzi.Landman@physics.gatech.edu

commutation or anticommutation relations

$$\begin{aligned} a_{j,\sigma}a_{k,\sigma'}^\dagger \mp e^{-i\theta \text{sgn}(j-k)}a_{k,\sigma'}^\dagger a_{j,\sigma} &= \delta_{j,k}\delta_{\sigma,\sigma'}, \\ a_{j,\sigma}a_{k,\sigma'} \mp e^{i\theta \text{sgn}(j-k)}a_{k,\sigma'}a_{j,\sigma} &= 0. \end{aligned} \quad (1)$$

The upper sign (commutation) applies for bosonic-based anyons; the lower sign (anticommutation) for fermionic-based anyons.  $\text{sgn}(j - k) = 1$  for  $j > k$ ,  $\text{sgn}(j - k) = -1$  for  $j < k$ , and  $\text{sgn}(j - k) = 0$  for  $j = k$ . For bosonic-based *spinless* anyons, one drops the spin index  $\sigma$ . On the same site, the two particles retain the usual bosonic or fermionic commutation relations.

*Case (i): Density-dependent Hubbard Hamiltonian for bosonic-based spinless anyons.* Adapting the many-site case of Refs. [24–26], a two-site anyonic Hubbard Hamiltonian for bosonic-based spinless anyons is written as follows:

$$H_{\text{spinless}} = -J(a_L^\dagger a_R + a_R^\dagger a_L) + \frac{U}{2} \sum_{j=L,R} n_j(n_j - 1), \quad (2)$$

where  $J$  is the tunneling parameter,  $U$  is the on-site interaction parameter (repulsive or attractive), and  $n_j = a_j^\dagger a_j$  is the number operator.

Using a fractional Jordan-Wigner transformation [24],

$$a_L = b_L \text{ and } a_R = b_R \exp(-i\theta n_L), \quad (3)$$

where  $b_j$  describes a usual bosonic operator and  $n_j = b_j^\dagger b_j = a_j^\dagger a_j$ , the anyonic Hamiltonian in Eq. (2) is mapped onto a bosonic Hubbard Hamiltonian with occupation-dependent hopping from right to left, i.e.,

$$H_{\text{spinless}}^B = -J(b_L^\dagger b_R e^{-i\theta n_L} + \text{h.c.}) + \frac{U}{2} \sum_{j=L}^R n_j(n_j - 1). \quad (4)$$

For two particles, if the left (target) site in unoccupied, the tunneling parameter is simply  $-J$ . If it is occupied by one boson, this parameter becomes  $-Je^{-i\theta}$ .

*Case (ii): Density-dependent Hubbard Hamiltonian for bosonic-based spin-1/2 anyons.* In this case, we introduce a two-site anyonic Hubbard Hamiltonian for bosonic-based spin-1/2 anyons as follows:

$$H_{\text{spin-1/2}}^B = -J \sum_\sigma (a_{L,\sigma}^\dagger a_{R,\sigma} + \text{h.c.}) + \frac{U}{2} \sum_{j=L,R} N_j(N_j - 1), \quad (5)$$

where  $N_j = \sum_\sigma a_{j,\sigma}^\dagger a_{j,\sigma}$ , with  $\sigma$  denoting the up ( $\uparrow$ ) or down ( $\downarrow$ ) spin;  $N_j$  is the number operator at each site  $j$  including the spin degree of freedom.

Using a modified fractional Jordan-Wigner transformation [30],

$$a_{L,\sigma} = b_{L,\sigma} \text{ and } a_{R,\sigma} = b_{R,\sigma} \exp(-i\theta N_L), \quad (6)$$

where  $b_{j,\sigma}$  describes a usual spin-1/2 bosonic operator and  $N_j = \sum_\sigma b_{j,\sigma}^\dagger b_{j,\sigma} = \sum_\sigma a_{j,\sigma}^\dagger a_{j,\sigma}$ , the anyonic Hamiltonian in Eq. (2) is mapped onto a bosonic Hubbard Hamiltonian with occupation-dependent hopping from right to left, i.e.,

$$\begin{aligned} H_{\text{spin-1/2}}^B = & -J \sum_\sigma (b_{L,\sigma}^\dagger b_{R,\sigma} e^{-i\theta N_L} + \text{h.c.}) + \frac{U}{2} \sum_{j=L,R} N_j(N_j - 1). \end{aligned} \quad (7)$$

For two particles, if the left (target) site in unoccupied, the tunneling parameter is simply  $-J$ . If it is occupied by one boson, this parameter becomes  $-Je^{-i\theta}$ .

*Case (iii): Density-dependent Hubbard Hamiltonian for fermionic-based spin-1/2 anyons.* In this case, we introduce a two-site anyonic Hubbard Hamiltonian for fermionic-based spin-1/2 anyons as follows:

$$H_{\text{spin-1/2}}^F = -J \sum_\sigma (a_{L,\sigma}^{F\dagger} a_{R,\sigma}^F + \text{h.c.}) + U n_{j,\uparrow}^F n_{j,\downarrow}^F, \quad (8)$$

where  $n_{j,\sigma}^F = a_{j,\sigma}^{F\dagger} a_{j,\sigma}^F$ , with  $\sigma$  denoting the up ( $\uparrow$ ) or down ( $\downarrow$ ) spin.

Using a modified fractional Jordan-Wigner transformation [30],

$$a_{L,\sigma}^F = f_{L,\sigma} \text{ and } a_{R,\sigma}^F = f_{R,\sigma} \exp(-i\theta N_L^F), \quad (9)$$

where  $f_{j,\sigma}$  describes a usual spin-1/2 fermionic operator and  $N_j^F = \sum_\sigma f_{j,\sigma}^\dagger f_{j,\sigma} = \sum_\sigma a_{j,\sigma}^{F\dagger} a_{j,\sigma}^F$ , the anyonic Hamiltonian in Eq. (2) is mapped onto a fermionic Hubbard Hamiltonian with occupation-dependent hopping from right to left, i.e.,

$$\begin{aligned} H_{\text{spin-1/2}}^F = & -J \sum_\sigma (f_{L,\sigma}^\dagger f_{R,\sigma} e^{-i\theta N_L^F} + \text{h.c.}) + U \sum_{j=L,R} U n_{j,\uparrow}^F n_{j,\downarrow}^F. \end{aligned} \quad (10)$$

For two particles, if the left (target) site in unoccupied, the tunneling parameter is simply  $-J$ . If it is occupied by one fermion, this parameter becomes  $-Je^{-i\theta}$ .

*Matrix representation of Hamiltonians:* In order to solve the two-site two-particle problem specified by the Hubbard-type Hamiltonians in Eqs. (4), (7), and (10), which have a density-dependent tunneling term, one needs to construct the corresponding matrix Hamiltonians. These matrices and the corresponding eigenenergies are presented below because for a finite number of particles they offer a better grasp of the role of the statistical angle  $\theta$ . The corresponding eigenvectors and other details of the derivation of the associated second-order momentum correlations and interferometry maps are given in the Appendices. When  $\theta = 0$ , these

Hamiltonian matrices reduce to the pure bosonic or fermionic two-trapped-particle interferometry problems; see Refs. [7, 8] for the pure fermionic interferometry case.

Using the bosonic basis kets

$$|2,0\rangle, |1,1\rangle, |0,2\rangle, \quad (11)$$

where  $|n_L, n_R\rangle$  (with  $n_L + n_R = 2$ ) corresponds to a permanent with  $n_L$  ( $n_R$ ) particles in the  $L$  ( $R$ ) site, one derives the following  $3 \times 3$  matrix Hamiltonian associated with the anyonic Hubbard Hamiltonian in Eq. (4)

$$H = \begin{pmatrix} U & -\sqrt{2}e^{-i\theta}J & 0 \\ -\sqrt{2}e^{i\theta}J & 0 & -\sqrt{2}J \\ 0 & -\sqrt{2}J & U \end{pmatrix}. \quad (12)$$

The three eigenenergies of the matrix (12) are given by

$$\begin{aligned} E_1 &= \frac{J}{2}(\mathcal{U} - \sqrt{\mathcal{U}^2 + 16}) \\ E_2 &= J\mathcal{U} = U \\ E_3 &= \frac{J}{2}(\mathcal{U} + \sqrt{\mathcal{U}^2 + 16}), \end{aligned} \quad (13)$$

where  $\mathcal{U} = U/J$ ; they are exact results and independent of the statistical angle  $\theta$ , unlike the mean-field energies [24]. (These eigenenergies are plotted in Fig. A1.) In contrast, the corresponding three normalized eigenvectors (see Appendices A and B) do depend on the statistical angle  $\theta$ . As explicitly shown below, this dependence results in tunable anyonic signatures that can be detected with controlled experimental protocols.

For the two spin-1/2 cases (whether for two bosons or fermions), we seek solutions for states with  $S_z = 0$  (vanishing total spin projection). In this case, the natural basis set is given by the four kets (note the choice of the ordering of these kets)

$$|\uparrow\downarrow, 0\rangle, |\downarrow, \uparrow\rangle, |\uparrow, \downarrow\rangle, |0, \uparrow\downarrow\rangle. \quad (14)$$

In first quantization, these kets correspond to permanents for bosons and to determinants for fermions. Employing this ket basis, one can derive the following  $4 \times 4$  matrix Hamiltonians associated with the spin-1/2 Hubbard Hamiltonians in Eqs. (7) and (10),

$$H = \begin{pmatrix} U & \mp e^{-i\theta}J & -e^{-i\theta}J & 0 \\ \mp e^{i\theta}J & 0 & 0 & \mp J \\ -e^{i\theta}J & 0 & 0 & -J \\ 0 & \mp J & -J & U \end{pmatrix} \quad (15)$$

where the upper minus sign in  $\mp$  applies for bosons and the bottom plus sign applies for fermions.

The four eigenenergies of the two matrices (15) are given by the three quantities  $E_i$ ,  $i = 1, \dots, 3$  in Eq. (13) and an additional vanishing eigenenergy  $E_4 = 0$ ; they are independent of the statistical angle  $\theta$  and the  $\mp$  alternation in sign. In contrast, as was also the case of

the spinless bosons, the corresponding four normalized eigenvectors do depend on the statistical angle  $\theta$ ; they are given in Appendices A and B.

*Second-order momentum correlation maps.* To generate the second-order momentum correlation maps  $\mathcal{G}^{S(A)}(k_1, k_2, \theta)$ , one needs to transit to the first-quantization formalism, which uses position- or momentum-dependent Wannier orbitals,  $\psi_L$  and  $\psi_R$ . Here and in the following, the superscripts  $S(A)$  denote symmetric (antisymmetric) behavior under the exchange of the momenta  $k_1$  and  $k_2$ . To this effect, each pure bosonic or fermionic particle in either of the two wells is represented by a displaced Gaussian function [7, 8], which equivalently in momentum space is given by

$$\psi_j(k) = \frac{2^{1/4}\sqrt{s}}{\pi^{1/4}}e^{-k^2s^2}e^{id_jk}, \quad (16)$$

where again the index  $j$  stands for  $L$  (left) or  $R$  (right); the separation between the two wells is  $2d = d_R - d_L$ .

The details of the derivation are given in Appendix C. Here we list the final analytical formulas for the  $\mathcal{G}(k_1, k_2)$ 's, which are independent of the total spin (i.e., whether the state is spinless or a spin singlet or a spin triplet state), and thus are the same for all three cases (i)-(iii). For the ground state, with energy  $E_1$ , one finds the following second-order momentum correlations

$$\begin{aligned} \mathcal{G}_1^S(k_1, k_2, \theta) &= \frac{2s^2e^{-2s^2(k_1^2+k_2^2)}}{\pi\sqrt{\mathcal{U}^2 + 16}} \times \\ &\left( \mathcal{R}(\mathcal{U})\cos^2[d(k_1 - k_2)] + \mathcal{R}(-\mathcal{U})\cos^2[d(k_1 + k_2) + \theta/2] + \right. \\ &\left. 8\cos[d(k_1 - k_2)]\cos[d(k_1 + k_2) + \theta/2]\cos(\theta/2) \right), \end{aligned} \quad (17)$$

where  $\mathcal{R}(\mathcal{U}) = \sqrt{\mathcal{U}^2 + 16} + \mathcal{U}$ .

For the excited state with energy  $E_2$ , one finds the following second-order momentum correlations

$$\mathcal{G}_2^S(k_1, k_2, \theta) = \frac{4s^2}{\pi}e^{-2s^2(k_1^2+k_2^2)}\sin^2[d(k_1 + k_2) + \theta/2]. \quad (18)$$

For the excited state with energy  $E_3$ , one finds the following second-order momentum correlations

$$\begin{aligned} \mathcal{G}_3^S(k_1, k_2, \theta) &= \frac{2s^2e^{-2s^2(k_1^2+k_2^2)}}{\pi\sqrt{\mathcal{U}^2 + 16}} \times \\ &\left( \mathcal{R}(-\mathcal{U})\cos^2[d(k_1 - k_2)] + \mathcal{R}(\mathcal{U})\cos^2[d(k_1 + k_2) + \theta/2] - \right. \\ &\left. 8\cos[d(k_1 - k_2)]\cos[d(k_1 + k_2) + \theta/2]\cos(\theta/2) \right), \end{aligned} \quad (19)$$

Finally, for the excited state with energy  $E_4$  [only for the two spin-1/2 cases (ii) and (iii)], one finds the following second-order momentum correlations

$$\mathcal{G}_4^A(k_1, k_2, \theta) = \frac{4s^2}{\pi}e^{-2s^2(k_1^2+k_2^2)}\sin^2[d(k_1 - k_2)]. \quad (20)$$

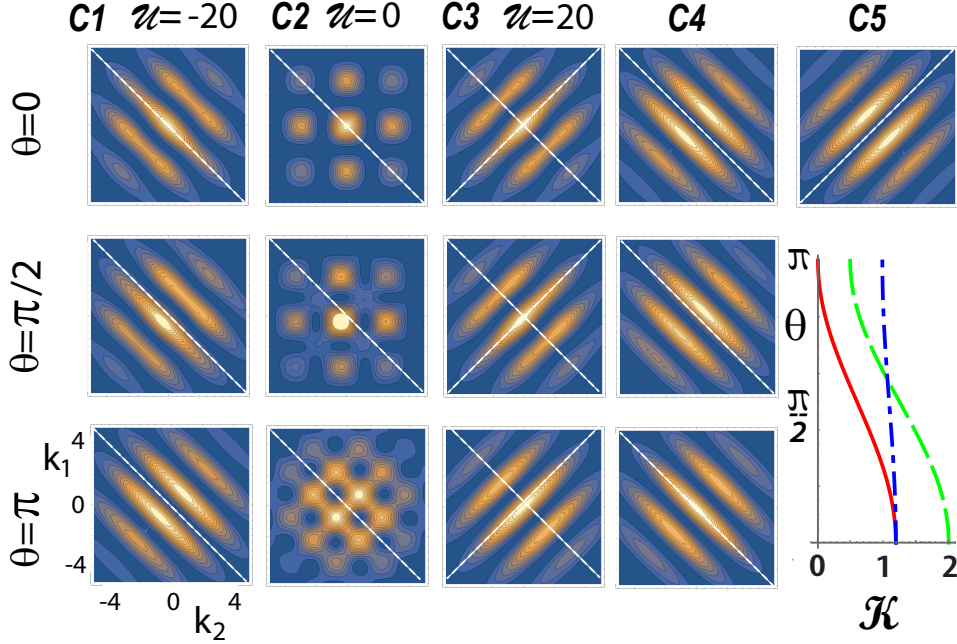


FIG. 1. Second-order momentum correlation maps exhibiting signatures of anyonic statistics (i.e., dependence on the statistical angle  $\theta$ ) for two interacting anyonic ultracold atoms trapped in a double well. Columns  $C1 - C3$ : case of the ground state (with energy  $E_1$ ) [see Eq. (17)], dependent on both the interaction  $\mathcal{U}$  and the statistical angle  $\theta$ . Column  $C1$ : strong attractive interparticle interaction  $\mathcal{U} = -20$ . Column  $C2$ : vanishing interparticle interaction,  $\mathcal{U} = 0$ . Column  $C3$ : strong repulsive interparticle interaction,  $\mathcal{U} = 20$ . Column  $C4$ : case of the excited state with energy  $E_2$  [see Eq. (18)], dependent on the statistical angle  $\theta$ , but independent of the interaction  $\mathcal{U}$ . Column  $C5$ , top frame: case of the excited state with energy  $E_4 = 0$  [see Eq. (20)], being independent from both  $\theta$  and  $\mathcal{U}$ ; this state is antisymmetric under the exchange of  $k_1$  and  $k_2$ . Column  $C5$ , bottom frame: The functions  $\mathcal{K}(\theta) = \pi \mathcal{G}_1^S(0, 0, \theta) / (4s^2)$  that correspond to Figs. 1(C1) (red solid line), Figs. 1(C2) (green dashed line), and Figs. 1(C3) (blue dash-dotted line) for the ground state. Top row:  $\theta = 0$  (pure bosons or fermions). Middle row:  $\theta = \pi/2$  (intermediate anyons). Bottom row:  $\theta = \pi$  (hard bosons or pseudofermions). The terms hard bosons and pseudofermions reflect the fact that the onsite commutation (anticommutation) relations do not change as a function of  $\theta$ , i.e., the onsite exclusion-principle behavior does not transmute from bosonic to fermionic and vice versa. The remaining parameters are: interwell distance,  $2d = 2 \mu\text{m}$  and width of single-particle orbital,  $s = 0.2 \mu\text{m}$ .  $k_1$  and  $k_2$  in units of  $1/\mu\text{m}$ . The dashed white lines are a guide to the eye. Blue represents the zero of the color scale. The white color corresponds to the maximum value of  $\mathcal{G}(k_1, k_2, \theta)$ .

The  $\mathcal{G}(k_1, k_2, \theta)$  expressions above exhibit the following properties: (1) The first three  $\mathcal{G}$ 's are symmetric under the exchange of the two momenta  $k_1$  and  $k_2$  and do depend on the statistical angle  $\theta$ . Thus their time-of-flight measurement will provide a signature for anyonic statistics. (2) The statistical angle  $\theta$  appears only in conjunction with cosine or sine terms containing the sum  $k_1 + k_2$  in their arguments. Cosine or sine terms containing only the difference  $k_1 - k_2$  of the two momenta are independent of  $\theta$ . This is a reflection of the fact that the vector solutions of the anyonic matrix Hamiltonians [see Eqs. (11) and (14)] contain the phase  $e^{i\theta}$  only in the NOON-state component [14–16] (of the form  $(|2, 0\rangle \pm e^{i\theta}|0, 2\rangle)/\sqrt{2}$  or  $|\uparrow\downarrow, 0\rangle \pm e^{i\theta}|0, \uparrow\downarrow\rangle$ , see Appendices), and not in the Einstein-Podolski-Rosen-state component [31] (of the form  $|1, 1\rangle$  or  $|\downarrow, \uparrow\rangle \pm |\uparrow, \downarrow\rangle$ ). (4) Only the fourth one associated with the constant energy  $E_4 = 0$  is antisymmetric under the exchange  $k_1$  and  $k_2$ . This state, which corresponds to two *indistinguishable* fermions (e.g., two  ${}^6\text{Li}$  atoms in a triplet excited state)

or bosons, is devoid of anyonic statistics.

Fig. 1 displays three cases (corresponding to the ground state and the two excited states with energies  $E_2$  and  $E_4$ ) of second-order momentum correlation maps that illustrate the above properties. The case of the excited state with energy  $E_3$  is presented in Fig. A2 of Appendix D. Keeping with property (2) above, the variation of the interference patterns as a function of  $\theta$  are more intense the larger the  $\mathcal{U}$ -dependent contribution of the  $k_1 + k_2$  terms in the total  $\mathcal{G}$  (the  $k_1 + k_2$  contributions produce interference fringes parallel to the antidiagonal). We note the alternation from a ridge to a valley along the antidiagonal in Fig. 1(C1) (ground state at attractive  $\mathcal{U} = -20$ ) and vice versa in Fig. 1(C4) ( $E_2$  state independent of  $\mathcal{U}$ ). For the ground state in the absence of interactions [Fig. 1(C2)], visible modifications (as a function of  $\theta$ ) of a plaid-type theme persist in the interference patterns. For the case when the  $k_1 + k_2$  terms have a small (or vanishing) contribution, the variations of the maps are minimal [see Fig. 1(C3)]

[or are absent, see Fig. 1(C5), top frame]; in this case, the dominance of the  $\theta$ -independent  $k_1 - k_2$  contributing terms is reflected in fringes parallel to the main diagonal. The bottom frame in the C5 column offers a complementary view of the  $\theta$  dependence by plotting the curves  $\mathcal{K}(\theta) = \pi\mathcal{G}_1^S(k_1 = 0, k_2 = 0, \theta)/(4s^2)$  that correspond to Figs. 1(C1), Figs. 1(C2), and Figs. 1(C3) for the ground state.

In summary, the paper introduced the subject of matter-wave interferometry of massive and interacting anyons that can be realized with trapped 1D ultracold atoms in optical lattices. Furthermore, it analyzed the pertinent signatures in the framework of time-of-flight experiments, and it established analogies with the interferometry of massless and noninteracting photonic anyons in waveguide lattices [14–16]. In particular, for two ultracold-atom anyons in a double-well confinement, this analogy is reflected in the fact that the NOON-state component of the massive bianyon is also of the form  $(|2, 0\rangle \pm e^{i\theta}|0, 2\rangle)/\sqrt{2}$ , where  $\theta$  is the statistical angle determining the commutation (anticommutation) relations for the anyonic exchange.

This work has been supported by a grant from the Air Force Office of Scientific Research (AFOSR, USA) under Award No. FA9550-15-1-0519. Calculations were carried out at the GATECH Center for Computational Materials Science.

### Appendix A: Solution for two bosonic-based spinless anyons

Using the bosonic basis kets

$$|2, 0\rangle, |1, 1\rangle, |0, 2\rangle, \quad (\text{A1})$$

where  $|n_L, n_R\rangle$  (with  $n_L + n_R = 2$ ) corresponds to a permanent with  $n_L$  ( $n_R$ ) particles in the  $L$  ( $R$ ) site, one derives the following matrix Hamiltonian associated with the anyonic Hubbard Hamiltonian in Eq. (4) of the main text

$$H = \begin{pmatrix} U & -\sqrt{2}e^{-i\theta}J & 0 \\ -\sqrt{2}e^{i\theta}J & 0 & -\sqrt{2}J \\ 0 & -\sqrt{2}J & U \end{pmatrix}. \quad (\text{A2})$$

The three eigenenergies of the matrix (A2) are given by

$$\begin{aligned} E_1 &= \frac{J}{2}(\mathcal{U} - \sqrt{\mathcal{U}^2 + 16}) \\ E_2 &= J\mathcal{U} = U \\ E_3 &= \frac{J}{2}(\mathcal{U} + \sqrt{\mathcal{U}^2 + 16}), \end{aligned} \quad (\text{A3})$$

where  $\mathcal{U} = U/J$ . These eigenenergies are plotted in Fig. A1.

The corresponding three normalized eigenvectors are

$$\begin{aligned} \mathcal{V}_1 &= \{\mathcal{B}(\mathcal{U})e^{-i\theta}/\sqrt{2}, \mathcal{A}(\mathcal{U}), \mathcal{B}(\mathcal{U})/\sqrt{2}\}^T \\ \mathcal{V}_2 &= \{e^{-i\theta}/\sqrt{2}, 0, -1/\sqrt{2}\}^T \\ \mathcal{V}_3 &= \{\mathcal{E}(\mathcal{U})e^{-i\theta}/\sqrt{2}, \mathcal{D}(\mathcal{U}), \mathcal{E}(\mathcal{U})/\sqrt{2}\}^T, \end{aligned} \quad (\text{A4})$$

where the coefficients  $\mathcal{A}$ ,  $\mathcal{B}$ ,  $\mathcal{D}$ , and  $\mathcal{E}$  are given by

$$\begin{aligned} \mathcal{A}(\mathcal{U}) &= \frac{\mathcal{U} + \sqrt{\mathcal{U}^2 + 16}}{\sqrt{2}\sqrt{\mathcal{U}^2 + \mathcal{U}\sqrt{\mathcal{U}^2 + 16} + 16}}, \\ \mathcal{B}(\mathcal{U}) &= \frac{4}{\sqrt{2}\sqrt{\mathcal{U}^2 + \mathcal{U}\sqrt{\mathcal{U}^2 + 16} + 16}}, \\ \mathcal{D}(\mathcal{U}) &= -\mathcal{A}(-\mathcal{U}), \\ \mathcal{E}(\mathcal{U}) &= \mathcal{B}(-\mathcal{U}). \end{aligned} \quad (\text{A5})$$

### Appendix B: Solution for two spin-1/2 anyons

We seek solutions for states with  $S_z = 0$  (vanishing total spin projection). In this case, the natural basis set is given by the four kets (note the choice of the ordering of these kets)

$$|\uparrow\downarrow, 0\rangle, |\downarrow\uparrow\rangle, |\uparrow,\downarrow\rangle, |0,\uparrow\downarrow\rangle. \quad (\text{B1})$$

In first quantization, these kets correspond to permanents for bosons and to determinants for fermions. Employing this basis, one can derive the following  $4 \times 4$  matrix Hamiltonians associated with the spin-1/2 Hubbard Hamiltonians in Eqs. (7) and (10) of the main text,

$$H = \begin{pmatrix} U & \mp e^{-i\theta}J & -e^{-i\theta}J & 0 \\ \mp e^{i\theta}J & 0 & 0 & \mp J \\ -e^{i\theta}J & 0 & 0 & -J \\ 0 & \mp J & -J & U \end{pmatrix} \quad (\text{B2})$$

where the upper minus sign in  $\mp$  applies for bosons and the bottom plus sign applies for fermions.

The four eigenenergies of the matrices (B2) are given by the quantities  $E_i$ ,  $i = 1, \dots, 3$  in Eq. (A3) and  $E_4 = 0$ ; they are independent of the  $\mp$  alternation in sign. The corresponding four normalized eigenvectors are

$$\begin{aligned} \mathcal{V}_1 &= \{\mathcal{B}(\mathcal{U})e^{-i\theta}/\sqrt{2}, \pm\mathcal{A}(\mathcal{U})/\sqrt{2}, \mathcal{A}(\mathcal{U})/\sqrt{2}, \mathcal{B}(\mathcal{U})/\sqrt{2}\}^T \\ \mathcal{V}_2 &= \{e^{-i\theta}/\sqrt{2}, 0, 0, -1/\sqrt{2}\}^T \\ \mathcal{V}_3 &= \{\mathcal{E}(\mathcal{U})e^{-i\theta}/\sqrt{2}, \pm\mathcal{D}(\mathcal{U})/\sqrt{2}, \mathcal{D}(\mathcal{U})/\sqrt{2}, \mathcal{E}(\mathcal{U})/\sqrt{2}\}^T \\ \mathcal{V}_4 &= \{0, 1/\sqrt{2}, \mp 1/\sqrt{2}, 0\}^T, \end{aligned} \quad (\text{B3})$$

where the upper sign (in  $\pm$  or  $\mp$ ) applies for bosons and the bottom sign applies for fermions.

### Appendix C: Second-order momentum correlation maps

To generate the second-order momentum correlation maps, one needs to transit from the ket notation to

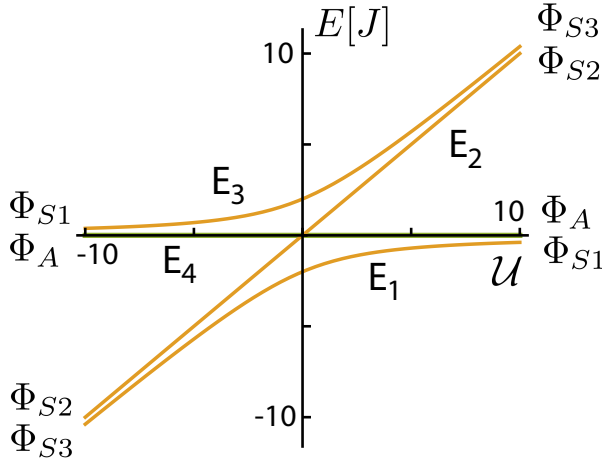


FIG. A1. Anyonic-Hubbard-dimer eigenenergies for all three cases of (i) spinless bosonic-based anyons, (ii) spin-1/2 bosonic-based anyons, and (iii) spin-1/2 fermionic-based anyons given by Eq. (A3) plus  $E_4 = 0$ . The limiting  $\Phi$  forms for the associated wave functions at  $\mathcal{U} \rightarrow \pm\infty$  are also denoted.

the wave function notation by employing the single-particle momentum-dependent Wannier orbitals  $\psi_L(k)$

and  $\psi_R(k)$  given in Eq. (16) of the main text. Indeed, in the first representation, the kets correspond to permanents for bosons or to determinants for fermions made of the  $\psi_L(k)$  and  $\psi_R(k)$  orbitals.

One finds the following correspondence for spinless anyons

$$\begin{aligned} |1, 1\rangle &\rightarrow \Phi_{S1}(k_1, k_2) \\ e^{-i\theta}|2, 0\rangle - |0, 2\rangle &\rightarrow \sqrt{2}\Phi_{S2}(k_1, k_2, \theta) \\ e^{-i\theta}|2, 0\rangle + |0, 2\rangle &\rightarrow \sqrt{2}\Phi_{S3}(k_1, k_2, \theta), \end{aligned} \quad (\text{C1})$$

and

$$\begin{aligned} |\uparrow, \downarrow\rangle \pm |\downarrow, \uparrow\rangle &\rightarrow \sqrt{2}\Phi_{S1}(k_1, k_2)\mathcal{X}_1 \\ e^{-i\theta}|\uparrow\downarrow, 0\rangle - |0, \uparrow\downarrow\rangle &\rightarrow \sqrt{2}\Phi_{S2}(k_1, k_2, \theta)\mathcal{X}_2 \\ e^{-i\theta}|\uparrow\downarrow, 0\rangle + |0, \uparrow\downarrow\rangle &\rightarrow \sqrt{2}\Phi_{S3}(k_1, k_2, \theta)\mathcal{X}_3 \\ |\uparrow, \downarrow\rangle \mp |\downarrow, \uparrow\rangle &\rightarrow \sqrt{2}\Phi_A(k_1, k_2)\mathcal{X}_4. \end{aligned} \quad (\text{C2})$$

for spin-1/2 anyons, where the upper sign applies to bosonic-based anyons and the bottom sign applies to fermionic-based ones.  $\mathcal{X}_i = \chi(1, 0)$  for  $i = 1, 2, 3$  and  $\mathcal{X}_4 = \chi(0, 0)$  for bosons and  $\mathcal{X}_i = \chi(0, 0)$ ,  $i = 1, 2, 3$  and  $\mathcal{X}_4 = \chi(1, 0)$  for fermions;  $\chi(0, 0)$  and  $\chi(1, 0)$  are the singlet and triplet spin eigenfunctions, respectively. The  $\Phi$  functions are as follows:

$$\begin{aligned} \Phi_{S1}(k_1, k_2) &= (\psi_L(k_1)\psi_R(k_2) + \psi_R(k_1)\psi_L(k_2))/\sqrt{2} = \frac{2s}{\sqrt{\pi}}e^{-s^2(k_1^2+k_2^2)}\cos[d(k_1 - k_2)], \\ \Phi_{S2}(k_1, k_2, \theta) &= (e^{-i\theta}\psi_L(k_1)\psi_L(k_2) - \psi_R(k_1)\psi_R(k_2))/\sqrt{2} = -i\frac{2s}{\sqrt{\pi}}e^{-s^2(k_1^2+k_2^2)}e^{-i\theta/2}\sin[d(k_1 + k_2) + \theta/2], \\ \Phi_{S3}(k_1, k_2, \theta) &= (e^{-i\theta}\psi_L(k_1)\psi_L(k_2) + \psi_R(k_1)\psi_R(k_2))/\sqrt{2} = \frac{2s}{\sqrt{\pi}}e^{-s^2(k_1^2+k_2^2)}e^{-i\theta/2}\cos[d(k_1 + k_2) + \theta/2], \\ \Phi_A(k_1, k_2) &= (\psi_L(k_1)\psi_R(k_2) - \psi_R(k_1)\psi_L(k_2))/\sqrt{2} = -i\frac{2s}{\sqrt{\pi}}e^{-s^2(k_1^2+k_2^2)}\sin[d(k_1 - k_2)]. \end{aligned} \quad (\text{C3})$$

For the ground state, with energy  $E_1$ , one finds the following second-order momentum correlations

$$\begin{aligned} \mathcal{G}_1^S(k_1, k_2, \theta) &= |\mathcal{A}(\mathcal{U})\Phi_{S1}(k_1, k_2) + \mathcal{B}(\mathcal{U})\Phi_{S3}(k_1, k_2, \theta)|^2 = \\ &\frac{4s^2}{\pi}e^{-2s^2(k_1^2+k_2^2)}\left(\mathcal{A}(\mathcal{U})^2\cos^2[d(k_1 - k_2)] + \mathcal{B}(\mathcal{U})^2\cos^2[d(k_1 + k_2) + \theta/2] + \right. \\ &\left. 2\mathcal{A}(\mathcal{U})\mathcal{B}(\mathcal{U})\cos[d(k_1 - k_2)]\cos[d(k_1 + k_2) + \theta/2]\cos(\theta/2)\right). \end{aligned} \quad (\text{C4})$$

For the excited state with energy  $E_2$ , one finds the following second-order momentum correlations

$$\mathcal{G}_2^S(k_1, k_2, \theta) = |\Phi_{S2}(k_1, k_2, \theta)|^2 = \frac{4s^2}{\pi}e^{-2s^2(k_1^2+k_2^2)}\sin^2[d(k_1 + k_2) + \theta/2]. \quad (\text{C5})$$

For the excited state with energy  $E_3$ , one finds the following second-order momentum correlations

$$\begin{aligned} \mathcal{G}_3^S(k_1, k_2, \theta) &= |-\mathcal{A}(-\mathcal{U})\Phi_{S1}(k_1, k_2) + \mathcal{B}(-\mathcal{U})\Phi_{S3}(k_1, k_2, \theta)|^2 = \\ &\frac{4s^2}{\pi}e^{-2s^2(k_1^2+k_2^2)}\left(\mathcal{A}(-\mathcal{U})^2\cos^2[d(k_1 - k_2)] + \mathcal{B}(-\mathcal{U})^2\cos^2[d(k_1 + k_2) + \theta/2] + \right. \\ &\left. - 2\mathcal{A}(-\mathcal{U})\mathcal{B}(-\mathcal{U})\cos[d(k_1 - k_2)]\cos[d(k_1 + k_2) + \theta/2]\cos(\theta/2)\right). \end{aligned} \quad (\text{C6})$$

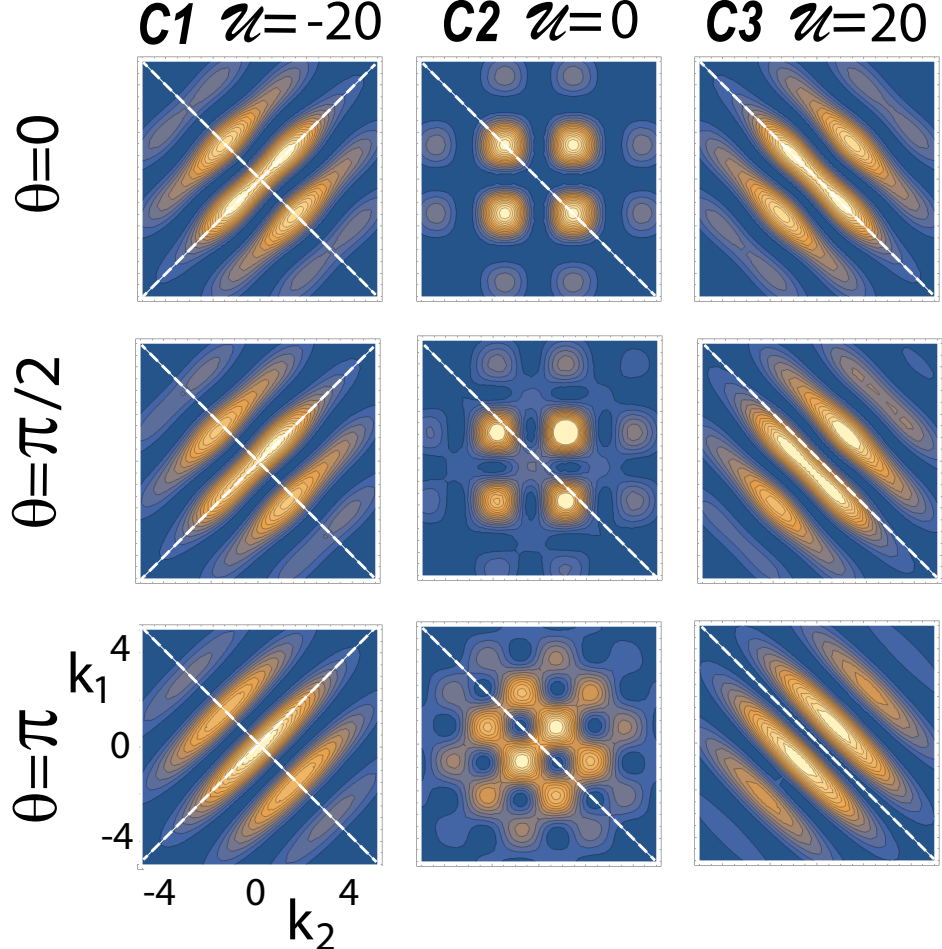


FIG. A2. Second-order momentum correlations of the excited state with energy  $E_3$  of two interacting anyonic ultracold atoms trapped in a double well [see Eq. (19) in the main text], demonstrating dependence on the statistical angle  $\theta$ . Top row:  $\theta = 0$  (pure bosons or fermions). Middle row:  $\theta = \pi/2$  (intermediate anyons). Bottom row:  $\theta = \pi$  (hard bosons or pseudofermions). Column C1: attractive interparticle interaction  $\mathcal{U} = -20$ . Column C2: vanishing interparticle interaction,  $\mathcal{U} = 0$ . Column C3: repulsive interparticle interaction,  $\mathcal{U} = 20$ . The remaining parameters are: interwell distance,  $2d = 2 \mu\text{m}$  and width of single-particle orbital,  $s = 0.2 \mu\text{m}$ .  $k_1$  and  $k_2$  in units of  $1/\mu\text{m}$ . The dashed white lines are a guide to the eye. Blue represents the zero of the color scale. The white color corresponds to the maximum value of  $\mathcal{G}_3^S(k_1, k_2, \theta)$ .

Finally, for the excited state with energy  $E_4 = 0$ , one finds the following second-order momentum correlations

$$\mathcal{G}^A(k_1, k_2, \theta) = |\Phi_A(k_1, k_2)|^2 = \frac{4s^2}{\pi} e^{-2s^2(k_1^2+k_2^2)} \sin^2[d(k_1 - k_2)]. \quad (\text{C7})$$

With regard to the derivation of the expressions in Eqs. (C4)–(C7), we note that, generally, the second-order (two-particle) space density  $\rho(x_1, x'_1, x_2, x'_2)$  for an  $N$ -particle system is defined as an integral over the product of the many-body wave function  $\Psi(x_1, x_2, \dots, x_N)$  and its complex conjugate  $\Psi^*(x'_1, x'_2, \dots, x_N)$ , taken over the coordinates  $x_3, \dots, x_N$  of  $N - 2$  particles. To obtain the second-order space correlation function,  $\mathcal{G}(x_1, x_2)$ , one

---

sets  $x'_1 = x_1$  and  $x'_2 = x_2$ . The second-order momentum correlation function  $\mathcal{G}(k_1, k_2)$  is obtained via a Fourier transform (from real space to momentum space) of the two-particle space density  $\rho(x_1, x'_1, x_2, x'_2)$  [7, 8]. In the case of  $N = 2$ , the above general definition reduces to a simple expression for the two-particle correlation functions, as the modulus square of the two-particle wave function itself; this applies in both cases whether the

two-particle wave function is written in space or in momentum coordinates. This simpler second approach was followed here for deriving above the second-order momentum correlations for two anyons.

#### Appendix D: Plots of correlation maps for the excited state with energy $E_3$

Fig. A2 displays the second-order correlation maps for the excited state with energy  $E_3$ . It complements Fig. 1 in the main text where the corresponding maps for the three eigenstates with energies  $E_1$ ,  $E_2$ , and  $E_4 = 0$  were displayed.

- 
- [1] I. Bloch, J. Dalibard, and W. Zwerger, Many-body physics with ultracold gases, *Rev. Mod. Phys.* **80**, 885 (2008).
- [2] J.I. Cirac and P. Zoller, Goals and opportunities in quantum simulation, *Nature Phys.* **8**, 264266 (2012).
- [3] S. Fölling, F. Gerbier, A. Widera, O. Mandel, T. Gericke, and I. Bloch, Spatial quantum noise interferometry in expanding ultracold atom clouds, *Nature* **434**, 491 (2005).
- [4] A.M. Kaufman, B.J. Lester, C.M. Reynolds, M.L. Wall, M. Foss-Feig, K.R.A. Hazzard, A.M. Rey, and C.A. Regal, Two-particle quantum interference in tunnel-coupled optical tweezers, *Science* **345**, 306 (2014).
- [5] R. Lopes, A. Imanaliev, A. Aspect, M. Cheneau, D. Boiron, and C.I. Westbrook, Atomic Hong-Ou-Mandel experiment, *Nature* **520**, 66 (2015).
- [6] R. Islam, R. Ma, Ph. M. Preiss, M.E. Tai, A. Lukin, M. Rispoli, and M. Greiner, Measuring entanglement entropy in a quantum many-body system, *Nature* **528**, 77 (2015).
- [7] B.B. Brandt, C. Yannouleas, and U. Landman, Two-point momentum correlations of few ultracold quasi-one-dimensional trapped fermions: Diffraction patterns, *Phys. Rev. A* **96**, 053632 (2017).
- [8] B.B. Brandt, C. Yannouleas, and U. Landman, Interatomic interaction effects on second-order momentum correlations and Hong-Ou-Mandel interference of double-well-trapped ultracold fermionic atoms, *Phys. Rev. A* **97**, 053601 (2018).
- [9] M. Bonneau, W.J. Munro, K. Nemoto, and Jörg Schmiedmayer, Characterizing twin-particle entanglement in double-well potentials, *Phys. Rev. A* **98**, 033608 (2018).
- [10] M.J. Hartmann, F.G.S.L. Brandao, and M.B. Plenio, Strongly interacting polaritons in coupled arrays of cavities, *Nat. Phys.* **2**, 849 (2006).
- [11] A.D. Greentree, C. Tahan, J.H. Cole, and L.C.L. Hollenberg, Quantum phase transitions of light, *Nat. Phys.* **2**, 856 (2006).
- [12] D.G. Angelakis, M.F. Santos, and S. Bose, Photonblockade-induced Mott transitions and XY spin models in coupled cavity arrays, *Phys. Rev. A* **76** 031805 (2007).
- [13] D. Rossini and R. Fazio, Mott-insulating and glassy phases of polaritons in 1D arrays of coupled cavities, *Phys. Rev. Lett.* **99**, 186401 (2007).
- [14] Y. Bromberg, Y. Lahini, and Y. Silberberg, Bloch oscillations of path-entangled photons, *Phys. Rev. Lett.* **105**, 263604 (2010).
- [15] S. Longhi and G. Della Valle, Anyons in one-dimensional lattices: a photonic realization, *Opt. Lett.* **37**, 2160 (2012).
- [16] M. Lebugle, M. Gräfe, R. Heilman, A. Perez-Leija, S. Nolte, and A. Szameit, Experimental observation of N00N state Bloch oscillations, *Nat. Commun.* **6**, 8273 (2015).
- [17] C. Noh and D.G. Angelakis, Quantum simulations and many-body physics with light, *Rep. Prog. Phys.* **80**, 016401 (2017).
- [18] J.M. Leinaas and J. Myrheim, On the theory of identical particles, *Il Nuovo Cimento B* **37**, 1 (1977).
- [19] F. Wilczek, Quantum mechanics of fractional-spin particles, *Phys. Rev. Lett.* **49**, 957 (1982).
- [20] A.Yu. Kitaev, Fault-tolerant quantum computation by anyons, *Ann. Phys. (N.Y.)* **303**, 2 (2003).
- [21] J.K. Pachos, *Introduction to topological quantum computation*, (Cambridge University Press, 2012)
- [22] T. Dubček, B. Klajn, R. Pezer, H. Buljan, and D. Jukić, Quasimomentum distribution and expansion of an anyonic gas, *Phys. Rev. A* **97**, 011601(R) (2018).
- [23] R.O. Umucalilar, E. Macaluso, T. Comparin, and I. Carusotto, Time-of-flight measurements as a possible method to observe anyonic statistics, *Phys. Rev. Lett.* **120**, 230403 (2018).
- [24] T. Keilmann, S. Lanzmich, I. McCulloch, and M. Roncaglia, Statistically induced phase transitions and anyons in 1D optical lattices, *Nat. Commun.* **2**, 361 (2011).
- [25] S. Greschner and L. Santos, Anyon Hubbard model in one-dimensional optical lattices, *Phys. Rev. Lett.* **115**, 053002 (2015).
- [26] Ch. Sträter, S.C.L. Srivastava, and A. Eckardt, Floquet realization and signatures of one-dimensional anyons in an optical lattice, *Phys. Rev. Lett.* **117**, 205303 (2016).
- [27] G. Tang, S. Eggert, and A. Pelster, Ground-state properties of anyons in a one-dimensional lattice, *New J. Phys.* **17**, 123016 (2015).
- [28] J. Arcila-Forero, R. Franco, and J. Silva-Valencia, Critical points of the anyon-Hubbard model, *Phys. Rev. A* **94**, 013611 (2016).
- [29] W. Zhang, S. Greschner, E. Fan, T.C. Scott, and Y. Zhang, Ground-state properties of the one-dimensional unconstrained pseudo-anyon Hubbard model, *Phys. Rev. A* **95**, 053614 (2017).
- [30] C.D. Batista and G. Ortiz, Algebraic approach to interacting quantum systems, *Adv. Phys.* **53**, 1 (2004).
- [31] Y.H. Shih, Entangled biphoton source - property and preparation, *Rep. Prog. Phys.* **66**, 1009 (2003).